Ligand Assisted Volatilization and Thermal Stability of $[(t\text{-BuN=})_2MoCl_2]_2$

*Michael A. Land,**,† *Katherine N. Robertson,*‡ *and Seán T. Barry*†

† Department of Chemistry, Carleton University, 1125 Colonel By Drive, Ottawa, Ontario K1S 5B6, Canada

‡ The Atlantic Centre for Green Chemistry, Department of Chemistry, Saint Mary's University, Halifax, Nova Scotia B3H 3C3, Canada

Abstract

Volatile molybdenum containing compounds have successfully been utilized for the atomic layer deposition of MoN_x, MoO_3, MoS_2, and MoC_xN_y. Most of the reported volatile molybdenum containing compounds have been prepared *via* salt metathesis reactions of *bis*(*tert*-butylimido)-dichloromolybdenum(VI), with anionic nitrogen based ligands. Herein we describe the preparation of several adducts of $[(t\text{-BuN=})_2MoCl_2]_2$ (**2**) *via* ligand exchange reactions with various neutral ligands, including both mono- and bidentate ethers, amines, and phosphines, as well as an *N*-heterocyclic carbene (NHC). These compounds have been characterized using NMR spectroscopy, elemental analysis, and the solid-state structures have been determined using single crystal X-ray crystallography. The volatility and thermal stability of all compounds have been assessed using TGA and DSC, showing that the coordinated ligands can improve the volatility, but in many cases the gas phase species reverts to **2**. This highlights a strategy for using coordinative ligands that are easily thermolyzed during evaporation and delivery yet improve the volatility of a key precursor.

Introduction

To keep pace with Moore's Law, the size regime of high-performance microelectronic component research and development has now shrunk to below 10 nm. When microelectronic interconnects – the wiring of integrated circuits – become smaller than 10 nm, the resistivity increases due to electromigration of the atoms within the interconnect metal. Promising metals to replace copper are molybdenum, osmium, iridium, ruthenium, rhodium, and tungsten. This is because they all have high melting temperatures, and relatively low bulk resistivities (~4-10 $\mu\Omega\cdot$cm), which both help prevent electromigration.[1,2] These potential interconnect metals can be deposited using atomic layer deposition (ALD): a stepwise, layer-by-layer, vapor phase, thin film deposition technique that produces uniform and high-quality thin films with atomic scale control.[3] ALD relies on volatile, inorganic and organometallic chemical precursors that react at specific surface nucleation points and that can then be chemically reduced to elemental metal films. The design and testing of potential precursors are a significant application of organometallic and inorganic compounds where thermal stability, volatility, and surface reactivity are important characteristics.[4]

While all of the aforementioned metals are potential alternatives for copper, most of the metals are either expensive (Ir, Rh, Ru), or have lasting toxic effects (Os). Therefore, the group VI elements are more interesting for development, with molybdenum being the focus herein. Currently, there are only two known processes for the ALD of molybdenum metal films. The first process was reported by the University of Helsinki in 1998 and uses $MoCl_5$ and zinc metal.[5] This method reports a growth per cycle of 0.8 Å and requires heating to 420 ºC, due to the low volatility of Zn.[5] The second known process for the ALD of Mo metal films uses MoF_6 and extremely hazardous Si_2H_6 as a coreactant.[6] This method, however, reports growths per cycle between 6 and 7 Å between 90 and 150 ºC;[6] these are very high growths for an ALD process. However, both of these processes produce films that contain a significant amount of impurities (Zn or Si, depending on the process) which lead to high resistivities.

Bis(*tert*-butylimido)-*bis*(dimethylamido)molybdenum(VI) is a volatile compound (reaching a vapor pressure of 1 Torr at 79 ºC).[7] It has been used as a precursor for the ALD of MoN_x,[8–11] MoO_3,[7,12–17] MoS_2,[18,19] and MoC_xN_y,[20] but it has not yet been reduced to molybdenum metal. This precursor is typically prepared from (t-BuN=)$_2$$MoCl_2$,[8] which is often isolated as the hexacoordinate 1,2-dimethoxyethane (dme) complex **1**.[21,22] Others have treated **1** with anionic *N*,*N'*-chelating ligands, such as guanidinates (which have yet to find success for Mo ALD),[23] and amidinates, which have recently been used, in conjunction with O_3, to prepare MoO_3 films.[24] Deposition of Mo metal from such compounds appears challenging, possibly due to the high nitrogen content in the ligands.

By far the majority of the investigations into the bisimido Mo(VI) systems for deposition precursors have focused on salt metathesis reactions of the dme adduct **1** to displace the chloride ligands. However, during routine thermal characterization we found that **1** was surprisingly volatile and had a good thermal stability (*vide infra*). To date, there are four crystallographically characterized bisimidodichloromolybdenum(VI) compounds that have incorporated neutral ligands other than dme. Two of those compounds are coordinatively saturated with THF, with very bulky aryl groups on the imido ligands.[25,26] The other two compounds are adducts of the (t-BuN=)$_2$$MoCl_2$ moiety and incorporate pyridine or *tert*-butylamine.[27] Both of the latter two compounds have been previously used for the low-pressure chemical vapor deposition of MoN_x and MoC_xN_y, but their thermal properties have yet to be assessed.[27] We decided to perform ligand exchange reactions to investigate the effect of various neutral coordinating ligands on the volatility and thermal stability of the (t-BuN=)$_2$$MoCl_2$ moiety. Herein we describe the synthesis and solid-state crystal structures for several coordination complexes of (t-BuN=)$_2$$MoCl_2$ with various neutral ligands, including both mono- and bidentate ethers, amines, and phosphines, as well as an *N*-heterocyclic carbene (NHC). Additionally, we discuss the volatility, thermal stability, and proposed mechanisms of decomposition of these compounds.

Results and Discussion

Synthesis and Characterization of Compounds

The known compound (t-BuN=)$_2$$MoCl_2$·dme **1** was prepared by oxo/imido-ligand exchange of sodium molybdate using *tert*-butylamine and triethylamine as an auxiliary base, followed by chlorination with chlorotrimethylsilane using Gibson's protocol (Scheme 1).[21] This compound was easily purified by recrystallization and the hitherto unknown solid-state structure of **1** was also determined using single-crystal X-ray diffraction (Figure 1, structural details discussed below).

Attempts to purify the dme adduct **1** by sublimation were unsuccessful, despite **1** exhibiting good volatility. Upon ^{1}H NMR analysis of the sublimate it was found that ~66% of the dme had been removed. This sublimate was then sublimed a second time and all the dme was removed. The spectroscopic characterization of this compound was not remarkable, exhibiting only a singlet in the ^{1}H NMR spectrum with a $\Delta\tau$ of -0.14 ppm for the *tert*-butylimido groups compared to those in **1**. X-ray quality crystals of this compound were obtained, and the solid-state structure revealed it to be a dimer of two (*t*-BuN=)$_2$MoCl$_2$ moieties, bridging through an imido group from each center (Figure 2). This is not surprising because a monomeric, tetracoordinate 12-electron (*t*-BuN=)$_2$MoCl$_2$ species should be unstable. The bulk composition of this dimeric compound, [(*t*-BuN=)$_2$MoCl$_2$]$_2$ **2** was also confirmed using elemental analysis. Additionally, the molecular ion for the monomeric unit, (*t*-BuN=)$_2$MoCl$_2$, has been detected using high-resolution electron-impact mass spectrometry: the dimer likely does not form a stable ion in the gas-phase.

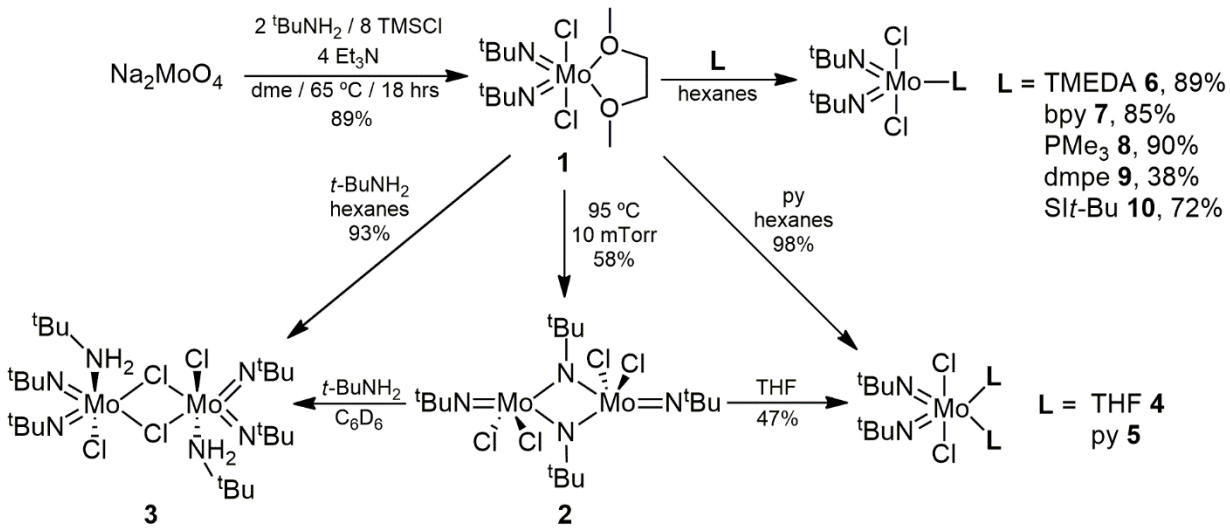

Scheme 1: Synthesis of the compounds discussed herein.

It should be noted that the chromium analogue, (*t*-BuN=)$_2$CrCl$_2$, has been characterized in the solid-state, and was found to be a monomer.[28,29] Additionally, the monomer (*t*-BuN=)$_2$MoCl$_2$ has been reported before,[30,31] synthesized using the relatively difficult to prepare MoO$_2$Cl$_2$ and *tert*-butylisocyanate. However, neither the solid-state structure nor the thermal properties were reported for this speculative species.[30,31] This led us to believe that the dimeric compound **2** could be prepared, in the absence of auxiliary ligands, under conditions similar to those used to synthesize **1**, except using benzene as a non-coordinating solvent. After sublimation of the crude product, it appeared that the dimeric compound **2** had been obtained, albeit in low yield. However, it was also contaminated with a second product which could not easily be removed. ^{1}H NMR showed this second compound to be the known [(*t*-BuN=)$_2$MoCl$_2$·(*t*-BuNH$_2$)]$_2$ **3**,[27] which incorporates *tert*-butylamine as a neutral ligand.[27] This was also confirmed by treating the mixture with *tert*-butylamine, resulting in the complete conversion of the dimer **2** to the *tert*-butyl adduct **3**. In the absence of a coordinating solvent, the (*t*-BuN=)$_2$MoCl$_2$ moiety was coordinatively saturated by *tert*-butylamine,[32] a reagent in the overall synthesis.

Ligands less Lewis basic than dme were added to solutions of **2** in attempts to isolate novel coordination complexes. Treatment of **2** with diethyl ether led only to the re-isolation of **2**, however when a similar reaction was carried out between **2** and THF, (*t*-BuN=)$_2$MoCl$_2$·(THF)$_2$ **4** was

isolated. Crystallography (Figure 1) and ^{1}H NMR spectroscopy suggest that two molecules of THF coordinate to the Mo center. The bulk purity of this compound could not be confirmed using elemental analysis: it appears to slowly liberate THF at room temperature, decomposing into a green solid. Using ^{1}H NMR the decomposition product appears to be the dimeric compound **2**, however, sub-stoichiometric amounts of THF were also observed.

With Lewis basic ligands more basic than dme, we were able to simply replace the dme in **1**. Initially we prepared the two known amine analogues, the *tert*-butylamine compound which exists as a bridging chloride dimer in the solid-state ($[(t\text{-BuN=})_2MoCl_2\cdot(t\text{-BuNH}_2)]_2$, **3**), and the *bis*-pyridine adduct ($(t\text{-BuN=})_2MoCl_2\cdot(py)_2$, **5**).[27] Synthesis of these compounds was achieved following known methods, by treating saturated hexane solutions of **1** with an excess of the amine, resulting in the immediate precipitation of the products in good yield. The identity of these compounds were confirmed using NMR spectroscopy, which was consistent with previous reports.[27]

Preparing the nitrogen-based chelate analogues of **1** was of interest since the chelate effect should stabilize these compounds with respect to thermolysis. The dme adduct **1** was treated directly with *N*,*N'*,*N'*-tetramethylethylenediamine (TMEDA) in hexanes and the analytically pure product, (t-BuN=)$_2$MoCl$_2$·TMEDA **6** was obtained in high yield after removal of the volatiles, including the displaced dme. It had previously been shown that the reaction between the dme adduct **1**, and 1,4,7-trimethyl-1,4,7-triazacyclononane resulted in an ionic salt, with the amine displacing one chloride ion.[33] In this case, such reactivity was not observed with TMEDA, and the covalent structure of **6** was confirmed using single-crystal X-ray crystallography (Figure 3). Additionally, the structure and bulk purity were further confirmed using NMR and elemental analysis, respectively. Another bidentate nitrogen-based ligand, 2,2'-bipyridine (bpy), was also added to **1** in hexanes resulting in the immediate precipitation of analytically pure (t-BuN=)$_2$MoCl$_2$·bpy **7**. This ligand was chosen because we thought that it would serve as an example of a ligand permitting less volatility than in **6** due to ligand π-stacking interactions (further discussed below). The bpy compound **7** had previously been reported; however, it was incompletely characterized, and its solid-state structure was hitherto unknown.[34] The ^{1}H NMR spectrum of this compound was more complex than the other compounds reported here because of long-range H−H coupling, as expected for a bpy adduct.

Our group has previously utilized trimethylphosphine as a ligand to prepare very volatile and thermally stable gold(I) precursors, therefore, we also chose to investigate it here.[35] Following the same protocol, trimethylphosphine was added directly to a hexanes solution of **1** and an off-white precipitate immediately formed. By ^{1}H NMR spectroscopy this compound appeared to be (t-BuN=)$_2$MoCl$_2$·PMe$_3$ **8**, containing only one PMe$_3$ ligand, despite having added more than two equivalents of phosphine. This compound was crystallographically characterized (Figure 4) and was confirmed to be the pentacoordinate Mo(VI) monomer compound in the solid-state. An electronic effect resulting from the highly Lewis basic PMe$_3$ ligand, likely reduces the Lewis acidity of the Mo center, which prevents formation of the *bis*-PMe$_3$ adduct. This suspicion is supported by the chemical shift of the *tert*-butylimido groups in the ^{1}H NMR spectrum, which were more shielded than those in the other compounds reported ($\Delta\tau$ = -0.24 ppm compared to **1**).

After finding that only one PMe$_3$ ligand was coordinated to the Mo center, we were curious if a phosphorus-based bidentate ligand could be employed. When the dme adduct **1** was treated with 1,2-*bis*(dimethylphosphino)ethane (dmpe) in hexanes, (t-BuN=)$_2$MoCl$_2$·dmpe **9** precipitated

immediately. This compound was only soluble in polar solvents, so solution phase characterization data was obtained in chloroform. The compound was also recrystallized from chloroform, which confirmed the structural connectivity and ensured that the product did not react with the solvent. The ^{1}H NMR spectrum of **9** suggested that the compound was asymmetric. It was initially thought that the dmpe was monodentate in solution, which would be consistent with the structure of the PMe_3 adduct **8**. However, the ^{13}C NMR spectrum revealed that the quaternary carbon atoms of the *tert*-butylimido groups were coupling to two phosphorus atoms, which would not be observed with a monodentate dmpe ligand. Finally, the solid-state structure of **9** revealed that the chloride ligands were *cis* to each other, whereas they are *trans* in the other hexacoordinate compounds described herein. This explains the observed asymmetry in the NMR spectra.

Our group has also successfully used using *N*-heterocyclic carbenes to drastically increase the thermal stability of group 11 precursors,[36–38] so we decided to use the same NHC as a coordination ligand for molybdenum. Freshly distilled 1,3-*bis*(*tert*-butyl)imidazolin-2-ylidene (SI*t*-Bu) was added dropwise to a hexanes solution of **1**. The anticipated product, (*t*-BuN=)$_2$MoCl$_2$·(SI*t*-Bu) **10** precipitated almost immediately as a pale yellow powder which was purified by recrystallization from toluene. The structure of this compound was determined using NMR, resulting in a shielding of the carbenic carbon atom in the ^{13}C NMR spectrum ($\Delta\tau$ = -6.3 ppm in C_6D_6).[39] The connectivity of **10** was also confirmed using X-ray crystallography, and a very long Mo−C bond was observed (discussed below, Figure 4). Finally, the bulk purity was confirmed using elemental analysis.

X-ray Crystallography

The solid-state structures for all of the compounds discussed, except for **3** and **5**, which have been reported previously,[27] were determined using single-crystal X-ray diffraction. Because all of the compounds described here are analogous, with the only difference being the neutral ligand, a summary of selected bond-lengths and angles is shown in Table 1. Additionally, relevant crystallographic parameters are provided in Table S2, and additional crystallographic images can also be found in the supporting information.

Table 1: Selected bond lengths and angles for the compounds studied.

Compound	Mo−N(*t*Bu) / Å	Mo−N−C(Me)$_3$ / °	Cl−Mo−Cl / °
1	1.7327(13) 1.7291(12)	162.37(11) 162.93(11)	158.94(3)
2	1.8010(10) 1.7214(11)	135.89(8) 167.80(8)	140.49(1)
3[27]	1.7366(25) 1.7253(25)	154.02(22) 172.42(23)	74.69(4) 86.16(4)
4	1.7539(15) 1.7242(18)	156.41(14) 170.5(2)	160.90(2)
5[27]	1.705(5) 1.736(4)	163.8(4) 173.4(4)	161.48(6)
6	1.7416(13) 1.7319(13)	159.62(11) 167.54(12)	165.77(2)
7	1.7473(12) 1.7419(10)	160.19(8) 169.32(11)	159.54(1)
8	1.7387(15)	166.87(13)	84.49(2)

	1.7353(15)	169.43(17)	
9	1.7553(14) 1.7488(15)	155.23(13) 178.85(12)	86.23(1)
10	1.734(3) 1.729(3)	148.5(2) 175.3(12)	157.51(4)

The results from the single crystal X-ray structural studies of the dme adduct **1** and the *bis*-ligated THF adduct **4** are shown in Figure 1, and due to their similarities they will be discussed together. The molybdenum centers were found to have octahedral geometries with the chloride ligands *trans* to each other in both structures (Table 1). The bond angles of the imido ligands suggest that there may be some additional electron donation (bond-order > 2) to the molybdenum center, which is further supported by the linear imido ligands (between 160 and 180°).[40] Other than very slight differences in the Mo−N−C(Me)$_3$ bond angles, the two structures overlay very well. Surprisingly, the oxygen atoms in both structures align almost perfectly, despite the bidentate dme ligand in **1** having less conformational freedom than the two monodentate ligands in **4**.

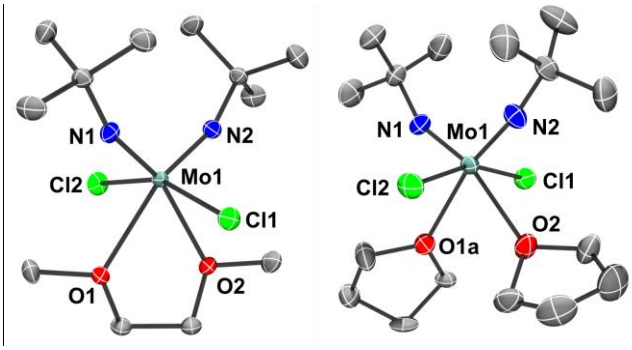

Figure 1: Solid-state structures of **1** (left) and **4** (right). Thermal ellipsoids are drawn at the 50% probability level. Hydrogen atoms have been omitted for visual clarity. The *tert*-butyl group (on N2) and the THF ligand (comprising O1) in **4** are disordered over two positions, however, only part A of the disorder is shown.

Compound **2** is a dimer in the solid state, bridging through one imido ligand of each monomeric Mo unit (Figure 2). The molybdenum centers exhibits a distorted geometry, between trigonal bipyramidal and square pyramidal (if the Mo−Mo bond is omitted; $\tau_5 = 0.49$).[41] The dimer is held together by unsymmetrically bridging imido ligands, nearly identical to those in the analogous structure, [(*t*-BuN=)$_2$MoMe$_2$]$_2$, reported by Nugent and Harlow.[42] This dimer also exhibits a short intramolecular interaction between the molybdenum atoms (3.0930(6) Å) which is below the sum of their covalent radii. Additionally, the dimer appears to be stabilized by C−H…Cl interactions between all of the chlorine atoms and methyl groups on the bridging *tert*-butylimido ligands, as well as C−H…N interactions between *tert*-butyl group of the bridging ligand and the nitrogen atom of the linear imido ligand (see Figure S50). Interestingly, this compound does not appear to have any short intermolecular interactions (below the sum of the Van der Waals radii), to other dimeric units.

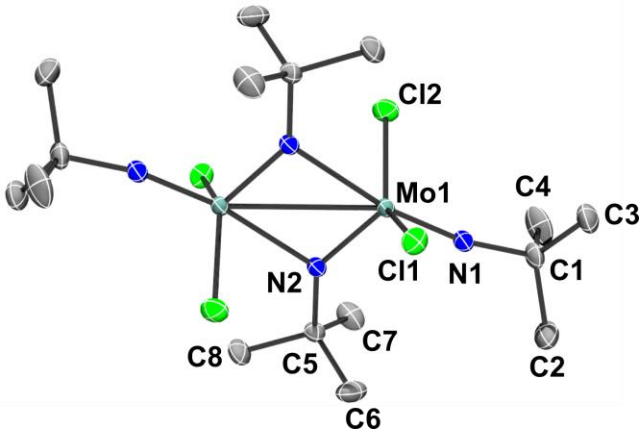

Figure 2: Solid-state structure of **2**. Thermal ellipsoids are drawn at the 50% probability level. Hydrogen atoms have been omitted for visual clarity. The other half of the dimer is generated by symmetry and only the crystallographically unique atoms are labeled.

The results from single-crystal X-ray diffraction studies for the two structures containing the bidentate nitrogen-based ligands, TMEDA **6** and bpy **7** (Figure 3), are very similar, therefore they will be discussed together. The molybdenum centers in both structures exhibit octahedral geometries with the chloride ligands *trans* to each other (Table 1). The two structures overlay very well despite one structure having a non-planar ligand (TMEDA, **6**), and the other having a planar ligand (bpy, **7**). The imido ligands in both structures also have very similar Mo−N−C(Me)$_3$ bond lengths (Table 1). One imido ligand in each structure is linear, suggesting some additional electron-donation from it to the metal.[40] The structure containing TMEDA **6** does not contain significant, short, intermolecular interactions. The structure containing bpy **7** contains several close *face-to-face* π-π stacking intermolecular interactions between the bpy fragments, and one *face-to-edge* interaction between the bpy ligand and a solvated benzene molecule (see Figure S53).

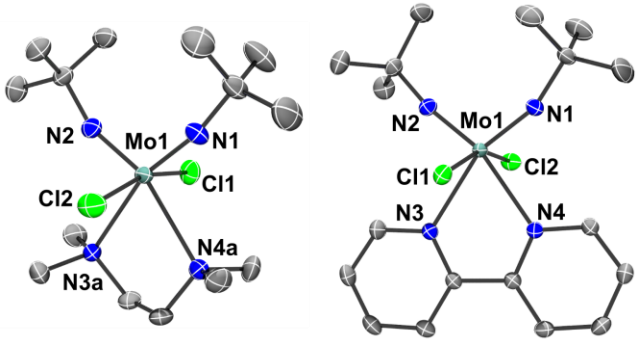

Figure 3: Solid-state structure of **6** (left) and **7** (right). Thermal ellipsoids are drawn at the 50% probability level. Hydrogen atoms have been omitted for visual clarity. The whole TMEDA ligand in **6** is disordered over two positions, however, only part A of the disorder is shown. The C_6H_6 solvate in **7** has also been omitted for visual clarity.

One might expect the structures of the compounds incorporating a phosphine ligand would be chemically similar to those that incorporate an NHC ligand, due to their similar electronic effects. However, the results of a single-crystal X-ray diffraction study revealed many differences, despite both **8** and **10** having pentacoordinate geometries (Figure 4). For example, the molybdenum atom in the PMe_3 adduct **8** exhibits a very distorted trigonal bipyramidal geometry (τ_5 = 0.62) whereas

the NHC adduct **10** exhibits a distorted square pyramidal geometry (τ_5 = 0.28).[41] However, the most striking difference between the two structures is that the chloride ligands are *cis* to each other in the PMe_3 adduct **8**, whereas they are *trans* to each other in the NHC adduct **10** (Table 1). Although phosphines and NHCs are good donors, one imido ligand in each of the two structures is linear. This suggests that there is additional electron donation from them,[40] likely because both of the structures are electron-deficient pentacoordinate complexes. Finally, neither structure exhibits any significant short intermolecular interactions, but the carbenic carbon atom forms a surprisingly long bond with the molybdenum center,[43] Mo−C7 = 2.414(4) Å, which is greater than the sum of the covalent radii of each atom.

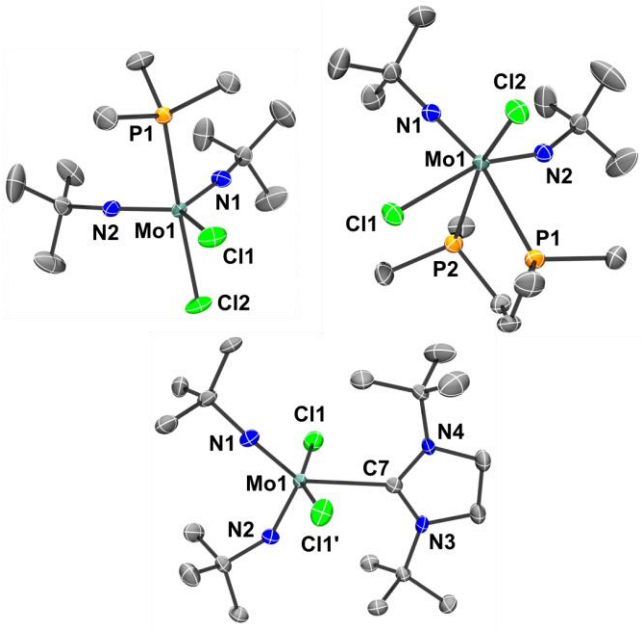

Figure 4: Solid-state structures of **8** (top left), **9** (top right), **10** (bottom). Thermal ellipsoids are drawn at the 50% probability level. Hydrogen atoms have been omitted for visual clarity. The *tert*-butyl group (on N2) in **8** and two *tert*-butyl groups (on N1 and N4) in **10** are disordered over two positions, however, only part A of the disorder is shown.

The final structure that was studied using X-ray crystallography is the dmpe adduct **9** (Figure 4). In the solid-state structure, the molybdenum center exhibits an octahedral geometry with the chloride ligands *cis* to each other (Table 1). In this structure it is obvious that one of the imido ligands is linear whereas the other is bent. Therefore, because compound **9** is hexacoordinate, and because phosphines are good donor ligands, this is the only structure described herein that may truly be an 18-electron structure.

Thermal Properties

For compounds to have merit as potential ALD candidates, they must have high thermal stability (high temperature of decomposition, T_D), and exhibit sufficient volatility (low temperature of volatilization, T_V). Additionally, the thermal range (ΔT; $T_D - T_V$) of these compounds must also be large, such that they can practically be used within ALD reactors. One method used to quantify the volatility of compounds is thermogravimetric analysis (TGA). In TGA a sample is heated and weighed at the same time and it can be used to determine how a compound volatilizes. For

example, thermally stable compounds show exponential mass-loss with increasing temperature, which can be described by an Arrhenius relationship.[44] Additionally, thermally stable compounds typically have a low or negligible residual mass, indicating that they have completely volatilized (without decomposition into non-volatile materials). It should be noted that low residual masses can still result from compounds that are not thermally stable but which decompose into compounds that are also volatile. For our purposes, this is not *necessarily* a pitfall, because it still means that volatile molybdenum-containing compounds are available for delivery into a deposition tool for film formation.

High residual mass from TGA can also provide some insight into the volatilization and decomposition of compounds. For example, if the residual mass percent is equivalent to the weight percent of molybdenum within the compound of study, it likely indicates that the compound decomposes into Mo metal. If the residual mass is above the weight percent of molybdenum it typically means that the compound has decomposed into a thermally stable product, with the most likely products being mixtures of molybdenum nitrides, carbides, and metal. Finally, low but non-negligible residual mass usually suggests that the compound volatilizes and decomposes at the same time. This observation can be further analyzed using a "thermal stress-test",[37,45] where the kinetics of evaporation are exploited. This is achieved by performing additional TGA experiments in which higher mass loadings are used while keeping a constant heating rate. If the compound is decomposing and evaporating at the same time, higher mass loadings will result in higher residual mass, because the material is "thermally stressed" as higher masses of material experience higher temperatures.

A standard definition for "volatility" of potential ALD precursors is the temperature where that compound reaches 1 Torr of vapor pressure. The vapor pressure can be estimated, based on the first derivative of the mass-loss curve from TGA data, using a previously reported model.[44] When we refer to T_V herein, we are referring to the temperature at which 1 Torr of vapor pressure has been achieved. All of the vapor pressure curves can be found in the supporting information.

To study the thermal stability and decomposition of potential precursors, we use differential scanning calorimetry (DSC, isochoric conditions) to complement TGA analyses (isobaric conditions). With DSC, the onset of thermal decomposition can be measured by an exothermic process, where the onset of decomposition (T_D) is defined as a 5% increase of the exothermic process. This value is arbitrarily chosen to compare all of the potential precursors. In many cases these decomposition products are non-volatile materials, and therefore if the compound decomposes, molybdenum is not readily available for deposition processes. The results of all these thermal analyses are tabulated below (Table 2).

Table 2: Important thermal properties obtained from TGA and DSC.

	T_V / ºC	T_D / ºC	ΔT / ºC	Residual mass / %	Figure of merit (σ)[a]
1	82	178	96	2.0	88
2	127	175	48	0.0	48
3	126	203	77	5.4	44
4	125	152	27	2.1	24
5	135	183	48	3.5	40
6	155	160	5	11.7	3

7	220	236	16	2.8	13
8	183	151	-32	2.8	-28
9	--[b]	108	--	29.9	--
10	165	167	2	8.6	1

[a] See Figure 9 for calculation;[36] the figure of merit is expressed in arbitrary units. [b] T_V could not be estimated for **9** due to multiple mass-loss events in the TGA.

First, the thermal behavior of the dme adduct **1** was investigated. Using thermogravimetric analysis, it was found that **1** volatilizes completely (Figure 5), resulting in a negligible residual mass. A large thermal range of 96 ºC was found before its onset of decomposition in the DSC (Table 2). Upon further investigations, it was found that the dme adduct **1** does not have a single mass-loss process, which is an indication of decomposition. When the heating rate of the TGA was reduced from the standard 10 ºC·min^{-1} to 5 ºC·min^{-1} two thermal events were clearly observed (Figure S2). Immediately after the first thermal event at 130 ºC, the remaining mass was 79%, which corresponded closely to the mass loss of dme from **1** (calcd. 77%). After this mass loss, the compound fully evaporates, resulting in a negligible residual mass. When the standard heating rate of 10 ºC·min^{-1} was employed (Figure 5), these two processes (dissociation of dme and the evaporation of the remaining mass) overlap, appearing to be a single thermal event. This corroborates our chosen synthesis of the dimeric compound **2**: it was prepared *via* the removal of dme from **1** during vacuum sublimation.

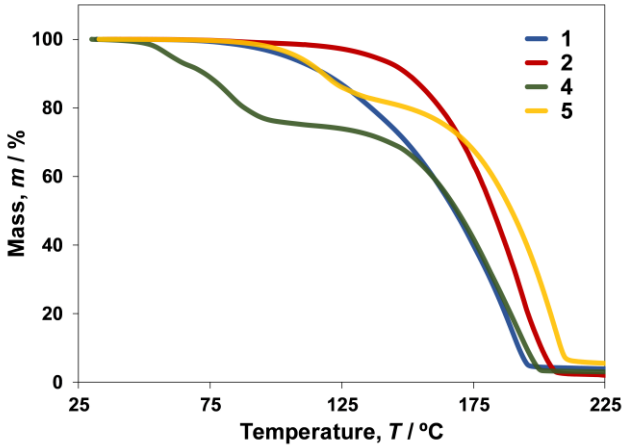

Figure 5: Thermogravimetric analyses of (*t*-BuN=)$_2$MoCl$_2$·dme **1** (blue), [(*t*-BuN=)$_2$MoCl$_2$]$_2$ **2** (red), (*t*-BuN=)$_2$MoCl$_2$·(THF)$_2$ **4** (green), and (*t*-BuN=)$_2$MoCl$_2$·(py)$_2$ **5** (yellow). A heating rate of 10 ºC·min^{-1} was used for all experiments, and the mass loadings were 10.0 ± 0.1 mg for each sample. The TGA curve for **1** is slightly obscured however it is also displayed in Figure 10.

Since the dimeric compound **2** is likely forming either prior to the volatilization of **1**, or in the gas-phase, the thermal properties of this compound were independently investigated. The TGA of dimeric compound **2** (Figure 5), shows that the onset of volatilization is higher than that of the dme adduct **1**. This is most likely because compound **2** is a dimer, and therefore has a higher molecular weight compared to **1**. Comparison of the vapor pressure curves for the dme adduct **1** and the dimeric compound **2** also shows that compound **2** is less volatile than **1** (Figure 6). The onset of decomposition of both compounds is equivalent, suggesting that **1** formed **2** in the sealed DSC pan, and the decomposition exotherm in both cases is that of **2** (Table 2). From these findings

we propose that the higher volatility of **1** results from "ligand-assisted volatilization" where the dme prevents the dimerization of the (*t*-BuN=)$_2$MoCl$_2$ moiety, thus increasing its volatility. However, the volatilization of both **1** and **2** yield the same gas-phase species. The larger thermal range of **1** can be exploited, provided that dme acts an innocent, spectator ligand during deposition processes.

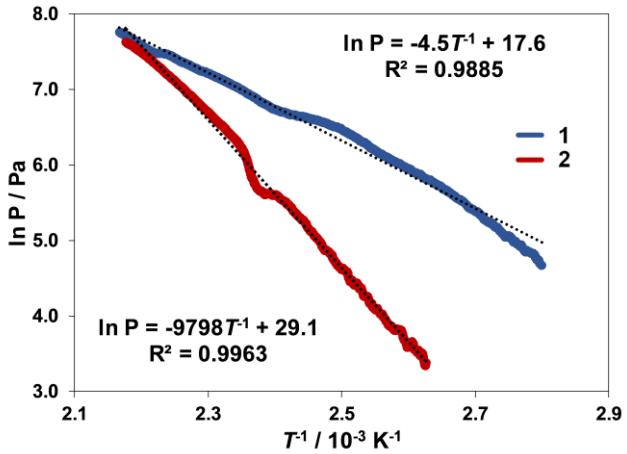

Figure 6: Vapor pressure of (*t*-BuN=)$_2$MoCl$_2$·dme **1** (blue) and [(*t*-BuN=)$_2$MoCl$_2$]$_2$ **2** (red) modeled according to the Langmuir equation estimated from TGA.[44]

We then measured the TGA and DSC behavior of the remaining compounds to investigate how different coordinating ligands change the thermal range of the "fundamental" dimer **2**. We expected two possible outcomes: 1) as with **1**, the ligands would dissociate from the molybdenum center at a low temperature, to further probe this idea of "ligand-assisted volatilization", or 2) the ligands would provide thermal stability, increasing the T_D of the new compound which would volatilize as a single species.

The known *bis*-pyridine adduct **5** had previously been reported to be a "volatile compound" for the chemical vapor deposition of molybdenum nitride and carbonitride, however, thermal data was not reported.[27] TGA of **5** showed a mass-loss event between 90 and 120 ºC resulting in a remaining mass of 82 % (Figure 5). This has been attributed to be the loss of pyridine (calculated loss of one pyridine ligand would result in 83% residual mass). Additionally, DSC showed an exothermic event at 109 ºC which corresponded to this pyridine dissociation (Figure S19). After the loss of one pyridine ligand, the compound appears to completely evaporate as a single species, with a very low residual mass. The estimated T_V of this product is equivalent to that of the dimeric compound **2** (Table 2).

The thermal properties of the analogous *bis*-THF adduct **4** were also studied, and it appeared to lose both THF ligands before 100 ºC, resulting in a remaining mass of 76 % (calcd. 68%). The compound appears to liberate THF even at room temperature, therefore some of the THF likely dissociated prior to TGA. Like the *bis*-pyridine adduct **5**, the *bis*-THF adduct **4** has the same T_V as the dimeric compound **2**. This similarity in volatility can also be observed in the overlay of the TGA curves (Figure 5), suggesting that compound **4** loses both of its THF ligands again forming the dimeric compound **2**.

Given that monodentate ligands appear to dissociate at low temperatures, we turned to bidentate ligands with the hope that the chelate effect would prevent this early dissociation. Although the TMEDA adduct **6** is most like the dme adduct **1** in connectivity, its TGA showed a high residual mass with an estimated T_V also significantly higher than that of the dme adduct **1** (Figure 7 and Table 2). The thermal range of compound **6** was also quite low as it appears to decompose prior to complete volatilization. It is unclear what might lead to this drastic difference, since both **1** and **6** have a similar molecular weight and the solid-state structures of both compounds are very similar, with neither exhibiting significant intermolecular interactions. The increased Lewis basicity of TMEDA compared to dme likely prevents the dissociation of TMEDA from **6** to form the dimeric compound **2**, which is likely the cause of the lower T_D. Although this compound has a high residual mass (11.7%), it is still lower than the weight percent of molybdenum in **6** (22.6%), indicating that some molybdenum-containing species did volatilize.

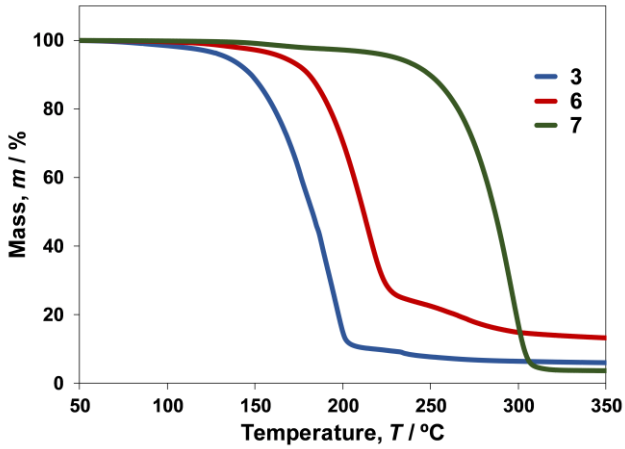

Figure 7: Thermogravimetric analyses of $[(t\text{-BuN=})_2MoCl_2\cdot(t\text{-BuNH}_2)]_2$ **3** (blue), $(t\text{-BuN=})_2MoCl_2\cdot$TMEDA **6** (red), and $(t\text{-BuN=})_2MoCl_2\cdot$bpy **7** (green). A heating rate of 10 °C·min^{-1} was used for all experiments, and the mass loadings were 10.0 ± 0.1 mg for each sample.

We predicted *a priori* that the incorporation of a bipyridine ligand into the $(t\text{-BuN=})_2MoCl_2$ system would serve as an example of how some ligands inhibit volatility through intermolecular interactions. However, initial inspection of the TGA curve of the bpy adduct **7** was quite surprising (Figure 7). Notably, it exhibited a single mass-loss curve and very low residual mass. It is true that the bpy adduct **7** exhibits significant π-π stacking interactions in the solid-state (Figures 3 and S53), which likely result in its high T_V (220 °C, Table 2). However, it was anticipated that **7** would decompose to yield a high residual mass; instead it appears to volatilize as a stable species. Notably, the onset of decomposition for **7** was significantly higher than all of the other reported compounds (Table 2). Despite the surprising results, it might make a suitable ALD precursor for a high-temperature process, although it has a small thermal range.

We investigated the thermal properties of the *tert*-butylamine adduct **3** because it had also been previously reported to be a "volatile compound" and was hitherto thermally characterized.[27] In an attempt to isolate the dimeric compound **2** in a non-coordinating solvent (discussed above), the *tert*-butylamine adduct **3** was isolated instead which showed that compound **3** was stable during sublimation (95 °C, 10 mTorr). The volatility of this compound can also be seen in the TGA curve (Figure 7). Compound **3**, however, did not completely volatilize before decomposition, based on

the residual mass of 5.4%, despite having a significantly higher T_D than compound **2**. Therefore, we speculate that compound **2** is more kinetically stable than **3** (*i.e.*, **3** decomposes faster than **2**).

From its TGA curve, the PMe_3 adduct **8** initially appeared promising showing a low residual mass (Figure 8). However, its thermal range was *negative*, with the onset of decomposition occurring before **8** can achieve a 1 Torr vapor pressure (Table 2). In one experiment, attempts were made to purify the PMe_3 adduct **8** *via* sublimation, however, the compound did not begin to sublime until 145 ºC (10 mTorr), and the resulting sublimate contained small amounts of unidentified decomposition products. In the ^{1}H NMR spectrum the relative integration of the sublimate was appropriate for **8**, suggesting that the phosphine does not dissociate from **8** upon sublimation; rather, it volatilizes as a single species very close to its T_D.

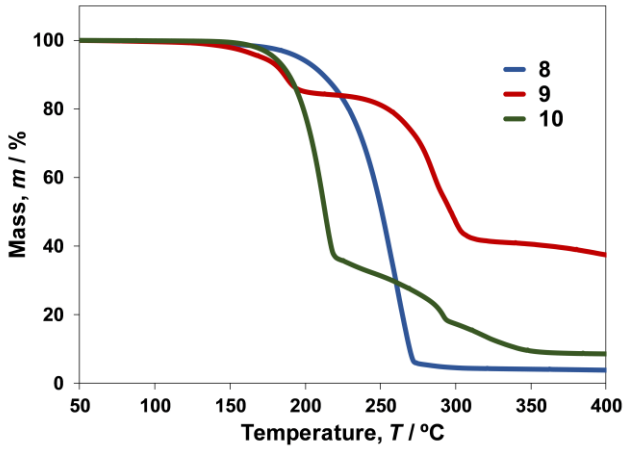

Figure 8: Thermogravimetric analyses of (*t*-BuN=)$_2$MoCl$_2$·PMe$_3$ **8** (blue), (*t*-BuN=)$_2$MoCl$_2$·dmpe **9** (red), and (*t*-BuN=)$_2$MoCl$_2$·(SI*t*-Bu) **10** (green). A heating rate of 10 ºC·min^{-1} was used for all experiments, and the mass loadings were 10.0 ± 0.1 mg for each sample.

We also investigated whether a bidentate phosphine would provide better stability than the monodentate ligand. The TGA curve of the dmpe adduct **9** demonstrated that it was not volatile (Figure 8). It exhibited multiple mass-loss events and had an extremely high residual mass (29.9%), higher than the calculated weight percent of molybdenum in **9** (20.9%). We speculate that the residual solid was likely a mixture of $MoCl_x$, MoN_x, and MoP_x based upon energy-dispersive X-ray spectroscopic (EDS) analysis of the residue (Figure S43). Since the TGA trace of **9** has multiple thermal events, a vapor pressure curve would not be genuine, therefore a T_V was not determined. Using DSC, the onset of decomposition of **9** was also significantly lower than in the other compounds discussed, it also corresponded well to the first mass-loss event observed by TGA. The first mass-loss results in a remaining mass of 85%, which we speculate to be due to the loss of one equivalent of isobutylene (calcd. 88%; discussed below). Isobutylene was observed by ^{1}H NMR following thermolysis of the dmpe adduct **9** in a flame-sealed NMR tube (Figure S38). Perhaps the *cis*-geometry of the chloride ligands promotes decomposition, or *cis*-geometry is a required intermediate configuration for decomposition. This theory is also supported by the bpy adduct **7** having *trans* chlorides and a significantly higher T_D.

The final compound to be discussed herein is the *N*-heterocyclic adduct **10**. Although NHCs are chemically similar to phosphines, their effect on volatility was notably different. This is not

surprising since NHCs are typically heavier than similar phosphines, and the solid-state structures of **8** and **10** were quite different (Figure 4). The TGA of **10** initially appeared promising, reaching a 1 Torr vapor pressure at a moderate temperature (Figure 8 and Table 2). However, the TGA exhibits a high residual mass (8.6%), below the weight percent of molybdenum in **10** (19.5%). Finally, although this NHC has been shown to significantly stabilize gold(I) compounds,[36] the T_D of the SI*t*-Bu adduct **10** was lower than that of the dimeric compound **2** (Table 2). This results in a negligible thermal range of 2 ºC.

The preceding data and analysis can be more easily visualized using a "figure of merit", σ. Our group has recently developed this statistic for comparing families of compounds (Figure 9).[36] The figure of merit is calculated according to the inset in Figure 9. The first term is the thermal range, which determines if a compound can achieve a 1 Torr vapor pressure before its onset of decomposition. The second term compares the residual mass to the weight percent of molybdenum in the compound. Thus, compounds will have a large σ when they have large thermal ranges and low residual masses. It cannot be used in cases where the T_V cannot be determined (like with **9**).

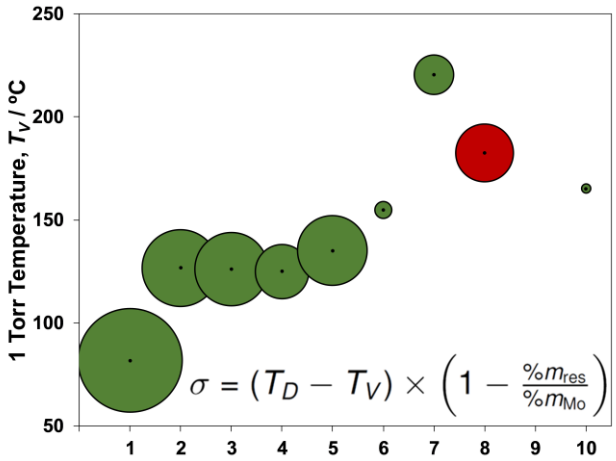

Figure 9: Figure of merit "minefield" diagram using data from Table 2. Green circles indicate a positive σ and red circles indicate a negative σ. The σ value of each compound is shown as the radius of each circle, in arbitrary units, centered at the compound's 1 Torr temperature, T_V.

The figure of merit can be visualized in a "minefield" diagram, where a point is plotted at the T_V of the compound and the radius of the circle is σ (Figure 9). This diagram basically summarizes all of the data described above (Table 2). For the family of compounds that has been studied herein, the greatest figure of merit belongs to the dme adduct **1**. Compounds **2**, **3**, and **5** also have good figure of merits with slightly higher T_V values. Due to its favorable σ, we studied the thermolysis of **1** further.

First, we performed a thermal "stress-test" to determine if the dme adduct **1** was kinetically stable at higher temperatures. As can be seen in Figure 10, the residual mass increased from 2% to 13% of the initial mass as the sample mass was increased from 10 to 55 mg. This suggests that not all of the material is able to evaporate before the decomposition temperature of 178 ºC. Therefore, although the dme adduct **1** decomposes at higher mass loadings, it can easily be integrated in deposition processes with delivery temperatures below 178 ºC (its T_D). The thermal "stress-test" of the dme adduct **1** showed a "ledge" at ~230 ºC that grew in with mass loading (denoted with a

* in Figure 10). This suggests that **1** decomposes into something that is not volatile and then further decomposes into another non-volatile material at 245 ºC. Although not observed until 230 ºC, this non-volatile species might be present at 178 ºC (T_D of **1**). The decomposition product could not be identified at lower mass loadings because most of the material had volatilized before it could reach these temperatures. The non-volatile decomposition products of **1** were examined by EDS and they qualitatively appear to be a mixture of $MoCl_x$ and MoN_x (Figure S40).

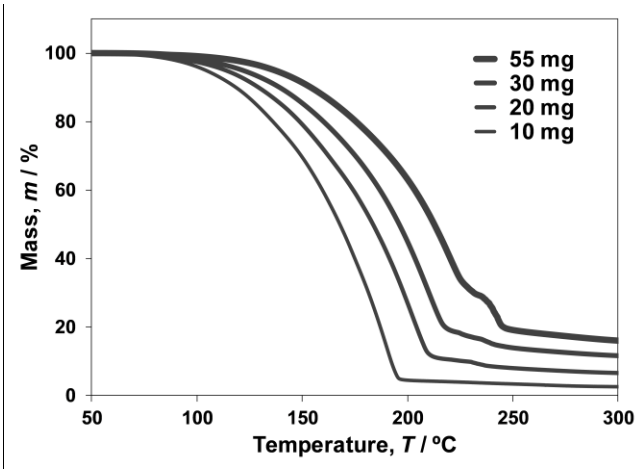

Figure 10: Thermal "stress-test" of (*t*-BuN=)$_2$MoCl$_2$·dme **1** using TGA showing an increased residual mass with higher initial mass loadings. The heating rate for all experiments was 10 ºC·min^{-1}.

To further study the thermal decomposition of the dme adduct **1**, solution phase thermolysis of compound **2** was undertaken. The dimeric compound **2** appears to be the product of the volatilization of **1**, and we wanted to prevent potential interference from dme in the solution phase. A deuterated-benzene solution of **2** was added to a thick-walled NMR tube which was subsequently flame-sealed. The NMR tube was then stored in an oven at 170 ºC. Using ^{1}H NMR spectroscopy, it was found that **2** had completely decomposed within 2 days at 170 ºC. Surprisingly, the ^{1}H NMR spectrum revealed one product, and only trace impurities were observed within the baseline (Figure S35). This product was determined to be isobutylene. The inside of the NMR tube was also coated with black-colored, insoluble solids (Figure S34).

A proposed mechanism for the thermal decomposition of **1** is shown in Scheme 2. We speculate that isobutylene forms *via* γ-hydrogen activation of the *tert*-butylimido ligands, a process which has previously been proposed for the decomposition of the *bis*-pyridine adduct **5**.[27] This would likely generate a protio-imido species **11**, which could further decompose into a polymeric species similar to **12**. ^{1}H NMR spectra were also collected periodically during the *in situ* thermolysis of the dimeric compound **2**, but a protio-imido species **11** could not be unambiguously identified, suggesting that it was a transient species in the decomposition. Although the final ^{1}H NMR spectrum clearly showed one product, the spectra collected during the thermolysis contained several different compounds, likely due to the multiple *tert*-butyl environments for various γ-H activation products. A compound analogous to **12** has previously been reported and it was found to only be soluble in liquid ammonia, which could explain why other decomposition products were be observed.[46] Additionally, a compound similar to **12** has been reported to decompose into a black residue at 250 ºC (similar to what was observed by TGA, Figure 10).[46]

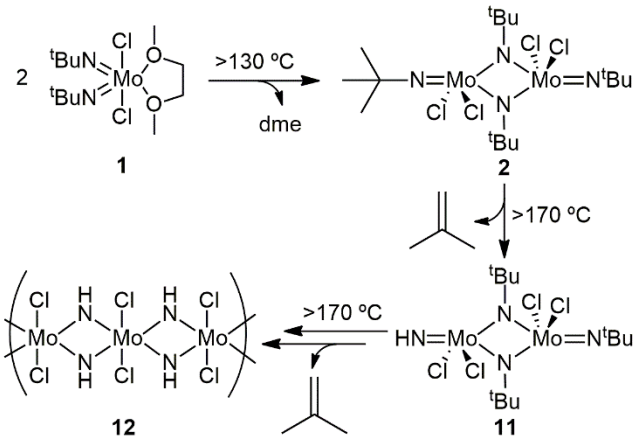

Scheme 2: Proposed thermal decomposition of (*t*-BuN=)$_2$MoCl$_2$·dme **1**.

Finally, the ^{1}H NMR spectra from the *in situ* thermolysis of the dimeric compound **2** was also used to obtain kinetics for its thermal decomposition in C_6D_6 at 170 ºC. A plot of the relative integration versus time (Figure S37) revealed linear relationships for the disapearance of **2** and the formation of isobutylene. This suggests that the decomposition is a zero order process, which is consistent with our proposed mechanism. It appears that most of the compounds described herein undergo similar decompositon pathways, where the neutral ligands likely dissociate at higher temperatures, forming **2**. The dmpe ligand would be expected to be one of the stronger ligands used, however, the dmpe adduct **9** has the lowest T_D. Therefore we speculate that the *cis*-chloride ligand geometry might activate a low-temperature thermal decomposition. The onset of decomposition of the other compounds (that do not lose their ligands) is higher because they first have to undergo *trans*-*cis* isomerization.

Conclusions

A series of *bis*(*tert*-butylimido)-dichloromolybdenum(VI) compounds, complexed by a variety of neutral ligands, were synthesized *via* ligand exchange reactions. These compounds were also structurally characterized using single crystal X-ray crystallography. The volatility of the compounds was studied using TGA. The dme adduct **1** was determined to be the most volatile with a vapor pressure of 1 Torr at 82 ºC. Additionally, some of these compounds appear to lose their ligands upon heating leading to the same coordinatively unsaturated compound **2**. The dimeric compound **2** is stabilized by dimerization in the solid phase, as determined by X-ray. The thermal stability of these compounds was assessed using DSC, with most of them exhibiting similar onset of decomposition temperatures (~170 ºC), with the exception of the bipyridine adduct **7** which is thermally stable to 236 ºC. For the most part it appears that these compounds decompose *via* γ-H activation, liberating isobutylene, as determined by NMR spectroscopy of the thermolysis in a sealed system. A figure of merit ranking system has been used to qualitatively compare various thermal properties of the compounds prepared herein. From this ranking system the compounds that should be candidates for further studies as potential precursors for ALD are the dme adduct **1**, the dimeric compound **2**, the *tert*-butylamine adduct **3**, and the *bis*-pyridine adduct **5**. Finally, strong donor ligands (such as phosphines and NHCs) do not improve the thermal behaviour of this system, likely because they prevent easy formation of **2** in the gas phase.

Experimental Section

Synthesis. *General Experimental.* All manipulations were performed under air-free conditions using either standard Schlenk techniques or in a nitrogen-filled (99.998% purity) MBraun glovebox. Sodium molybdate (≥98%), triethylamine (≥99%), chlorotrimethylsilane (≥98%), *tert*-butylamine (98%), *N,N,N′,N′*-tetramethylethylenediamine (99%), 2,2'-bipyridine (≥99%), and pyridine (99.8%) were purchased from Sigma-Aldrich and were used as received. Trimethylphosphine (98%), and 1,2-*bis*(dimethylphosphino)ethane (98%) were purchased from Strem Chemicals Inc. and were used as received. $[(t\text{-BuN=})_2MoCl_2\cdot(t\text{-BuNH}_2)]_2$ **3**, and $(t\text{-BuN=})_2MoCl_2\cdot(py)_2$ **5** were prepared from **1** and the corresponding amine, according to a previously reported method.[27] 1,3-*Bis*(*tert*-butyl)imidazolin-2-ylidene (SI*t*-Bu) was also prepared following a known method.[39] All solvents (ACS reagent-grade) were purified using a MBraun Solvent Purification System and were stored over 4 Å molecular sieves. All glassware was oven-dried at 130 ºC, for at least 3 hours, prior to use. NMR spectra were collected at room temperature in either C_6D_6 or $CDCl_3$ on a Bruker AVANCE 300 MHz spectrometer and were referenced to residual solvent. C_6D_6 was purchased from Sigma-Aldrich, and $CDCl_3$ was purchased from Alfa Aesar. Both deuterated solvents were degassed using freeze-pump-thaw cycles and were stored over 4 Å molecular sieves under nitrogen. Elemental analyses (EA) were performed on a Perkin Elmer Series II CHN Analyser at the Centre for Environmental Analysis and Remediation (CEAR) at Saint Mary's University. The EA samples were prepared in a glovebox, using 3.500 ± 1 mg of material, and cystine was used for the standard calibration.

$(t\text{-BuN=})_2MoCl_2\cdot$dme ***1***. Synthesis followed known methods.[21,22] Sodium molybdate (10.014 g, 48.631 mmol) was suspended in 150 mL of 1,2-dimethoxyethane. Triethylamine (27 mL, 194 mmol), chlorotrimethylsilane (56 mL, 441 mmol), and *tert*-butylamine (12 mL, 114 mmol) were added to the suspension sequentially and the mixture was heated to reflux, under nitrogen, for 24 hours. The resulting dark-yellow suspension was filtered through a sintered-glass frit, and the residual solids were washed with pentane until they were white (three, 10 mL portions). The volatiles of the filtrate were then removed *in vacuo* resulting in dark-yellow/beige colored solids. The product was extracted with three, 100 mL portions of hexanes and the volatiles were removed *in vacuo* resulting in analytically pure material. Yield = 17.319 g (43.381 mmol, 89%). X-ray quality crystals were obtained after storing a saturated pentane solution at -30 ºC for 24 hours. Spectroscopic data was consistent with that reported previously:[21,22] ^{1}H NMR (300 MHz, C_6D_6, ppm): δ 1.42 (s, 18H, C(C*H*$_3$)$_3$), 3.22 (s, 4H, OC*H*$_2$), 3.48 (s, 6H, OC*H*$_3$). ^{13}C{^{1}H} NMR (75 MHz, C_6D_6, ppm): δ 30.20 (C(*C*H$_3$)$_3$), 62.69 (O*C*H$_2$), 70.66 (O*C*H$_3$), 71.80 (*C*(CH$_3$)$_3$).

$[(t\text{-BuN=})_2MoCl_2]_2$ ***2***. The product was obtained *via* the removal of dme from **1**. First, the dme complex **1** (1.435 g, 3.596 mmol) was added to a sublimation apparatus, with a water-cooled cold-finger. The compound was sublimed (95 ºC, 10 mTorr) and 1.068 g of an orange solid was isolated. ^{1}H NMR analysis revealed that ~66% of the dme had been removed. This material was then collected, and the product was re-sublimed under the same conditions. This also resulted in an orange solid and ^{1}H NMR analysis revealed that almost all of the dme had been removed (~99%), and the product was determined to be pure enough for further investigations. Yield = 0.648 g (1.049 mmol, 58%). ^{1}H NMR (300 MHz, C_6D_6, ppm): δ 1.28 (s, 36H, C(C*H*$_3$)$_3$). ^{13}C{^{1}H} NMR (75 MHz, C_6D_6, ppm): δ 30.09 (C(*C*H$_3$)$_3$), 74.33 (*C*(CH$_3$)$_3$). EA calcd for $C_{16}H_{36}Cl_4Mo_2N_4$ [%]: C, 31.08; H, 5.87; N, 9.06; found [%]: C, 31.37; H, 5.85; N, 9.01. HRMS (EI) calcd for $[C_8H_{18}Cl_2MoN_2]^+$: *m/z* = 303.99151; found: *m/z* = 303.98927, dev. -1.74 mmu.

(t-BuN=)$_2$MoCl$_2$·(THF)$_2$ ***4***. The dimeric compound **2** (0.168 g, 0.272 mmol) was dissolved in 2 mL of THF and 3 mL of pentane, in a 20-mL scintillation vial. The mixture was stirred at room temperature for 2 hours and then the uncapped vial was placed in a sealed, nitrogen-filled 250-mL glass jar. The product was isolated *via* slow evaporation of the solvent over three days. This resulted in thin yellow plate-like crystals. Yield = 0.116 g (0.256 mmol, 47%). ^{1}H NMR (300 MHz, C_6D_6, ppm): δ 1.34-1.39 (m, 8H, OCH$_2$C*H*$_2$), 1.40 (s, 18H, C(C*H*$_3$)$_3$), 3.73-3.80 (m, 8H, OC*H*$_2$CH$_2$). ^{13}C{^{1}H} NMR (75 MHz, C_6D_6, ppm): δ 25.77 (OCH$_2$*C*H$_2$), 30.08 (C(*C*H$_3$)$_3$), 69.11 (O*C*H$_2$CH$_2$), 69.33 (*C*(CH$_3$)$_3$). This compound slowly turned orange, then green, at room temperature liberating THF; additionally, the compound could not be dried *in vacuo*, therefore, adequate EA could not be obtained. EA calcd for $C_{16}H_{34}Cl_2MoN_2O_2$ [%]: C, 42.39; H, 7.56; N, 6.18; found [%]: C, 35.44; H, 6.53; N, 8.00.

(t-BuN=)$_2$MoCl$_2$·TMEDA ***6***. *N,N,N',N'*-tetramethylethylenediamine (0.100 mL, 0.668 mmol) was added to a solution of **1** (0.240 g, 0.601 mmol) in 10 mL of hexanes. A precipitate was not immediately observed, therefore, the mixture was stirred for 12 hours to ensure completion. The volatiles were removed *in vacuo* resulting in a dark-yellow powder, of analytically pure **6**. Yield = 0.227 g (0.534 mmol, 89%). X-ray quality crystals were obtained from storing a saturated hexanes solution at -30 ºC for 24 hours. ^{1}H NMR (300 MHz, C_6D_6, ppm): δ 1.43 (s, 18H, C(C*H*$_3$)$_3$), 2.09 (s, 4H, NC*H*$_2$), 2.57 (s, 12H, N(C*H*$_3$)$_2$). ^{13}C{^{1}H} NMR (75 MHz, C_6D_6, ppm): δ 30.09 (C(*C*H$_3$)$_3$), 50.60 (N(*C*H$_3$)$_2$), 57.19 (N*C*H$_2$), 71.49 (*C*(CH$_3$)$_3$). EA calcd for $C_{14}H_{34}Cl_2MoN_4$ [%]: C, 39.54; H, 8.06; N, 13.17; found [%]: C, 39.47; H, 8.09; N, 13.04.

(t-BuN=)$_2$MoCl$_2$·bpy ***7***. 2,2'-Bipyridine (0.071 g, 0.455 mmol) was added to a solution of **1** (0.190 g, 0.476 mmol) in 8 mL of pentane, resulting in a pale-yellow suspension. The mixture was stirred for 1 hour to ensure complete reaction. The supernate was decanted and the solids were washed with three, 2 mL portions of pentane. The solids were then dried *in vacuo* resulting in a pale-yellow powder of analytically pure **7**. Yield = 0.181 g (0.389 mmol, 85%). X-ray quality crystals of **7**·$(C_6H_6)_{1.5}$ formed in the bottom of an NMR tube overnight. ^{1}H NMR (300 MHz, C_6D_6, ppm): δ 1.70 (s, 18H, C(C*H*$_3$)$_3$), 6.65 (dd, 1H, *J* = 5.3 & 1.2 Hz), 6.68 (dd, 1H, *J* = 5.3 & 1.1 Hz), 6.90 (td, 2H, *J* = 7.7 & 1.8 Hz), 7.08 (d, 2H, *J* = 8.0 Hz), 9.56 (dq, 2H, *J* = 5.3 & 0.8 Hz). ^{13}C{^{1}H} NMR (75 MHz, C_6D_6, ppm): δ 30.86 (C(*C*H$_3$)$_3$), 71.40 (*C*(CH$_3$)$_3$), 121.49, 124.81, 138.18, 150.88, 152.80. EA calcd for $C_{18}H_{26}Cl_2MoN_4$ [%]: C, 46.46; H, 5.63; N, 12.04; found [%]: C, 46.37; H, 5.68; N, 11.96.

(t-BuN=)$_2$MoCl$_2$·PMe$_3$ ***8***. Trimethylphosphine (0.110 mL, 1.081 mmol) was added to a solution of **1** (0.338 g, 0.847 mmol) in 10 mL of hexanes resulting in the formation of an off-white precipitate. The mixture was stirred for 2 hours and the volatiles were removed *in vacuo* and the resulting off-white solids were washed with three, 2 mL portions of pentane. The solids were then dissolved in 3 mL of toluene and 3 mL dichloromethane and the solution was layered with 2 mL of pentane. The mixture was stored at -30 ºC for 18 hours. The product **8** was isolated as an analytically pure yellow powder after decanting the supernate and drying the powder *in vacuo*. Yield = 0.292 g (0.758 mmol, 90%). X-ray quality crystals were obtained after storing a saturated acetonitrile solution, layered with pentane, at -30 ºC for 24 hours. ^{1}H NMR (300 MHz, C_6D_6, ppm): δ 1.08 (d, 9H, $^2J_{PH}$ = 10.2 Hz, P(C*H*$_3$)$_3$), 1.18 (s, 18H, C(C*H*$_3$)$_3$). ^{13}C{^{1}H} NMR (75 MHz, C_6D_6, ppm): δ 16.29 (d, $^1J_{CP}$ = 29.7 Hz, P(*C*H$_3$)$_3$), 30.75 (d, $^4J_{CP}$ = 2.4 Hz, C(*C*H$_3$)$_3$), 72.19 (d, $^3J_{CP}$ = 3.3 Hz, *C*(CH$_3$)$_3$). ^{31}P{^{1}H} NMR (121 MHz, C_6D_6, ppm): δ 4.49 (s, *P*(CH$_3$)$_3$). EA calcd for $C_{11}H_{27}Cl_2MoN_2P$ [%]: C, 34.30; H, 7.07; N, 7.27; found [%]: C, 34.68; H, 7.08; N, 7.35.

(t-BuN=)$_2$MoCl$_2$·dmpe ***9***. A solution of **1** (0.295 g, 0.739 mmol) in 10 mL of hexanes was added dropwise to a solution of 1,2-*bis*(dimethylphosphino)ethane (0.140 mL, 0.839 mmol) in 3 mL of hexanes. The mixture was stirred for 2 hours, resulting in an orange precipitate. The supernate was decanted and the solids were washed with three, 2 mL portions of pentane and three, 2 mL portions of toluene. The material was then dissolved in 3 mL of chloroform and was triturated with 10 mL of pentane. A viscous dark-colored oil formed on the bottom of the vial, and a semi-crystalline orange material began to precipitate from solution. The mixture was quickly transferred to another vial (leaving the dark-colored oil stuck to the bottom of the first vial) and was stored at -30 ºC for 18 hours resulting in bright orange crystals. The supernate was decanted and the product was dried *in vacuo*. Yield = 0.128 g (0.279 mmol, 38%). This compound was only sparingly solubility in C_6D_6. ^{1}H NMR (300 MHz, $CDCl_3$, ppm): δ 1.42 (s, 18H, C(C*H*$_3$)$_3$), 1.55 (d, 6H, $^2J_{PH}$ = 8.3 Hz, P(C*H*$_3$)$_2$), 1.72 (d, 6H, $^2J_{PH}$ = 10.2 Hz, P(C*H*$_3$)$_2$), 1.95-2.29 (m, 4H, PC*H*$_2$). ^{13}C{^{1}H} NMR (75 MHz, $CDCl_3$, ppm): δ 12.36 (d, $^1J_{CP}$ = 15.7 Hz, P(*C*H$_3$)$_2$), 17.71 (d, $^1J_{CP}$ = 28.5 Hz, P(*C*H$_3$)$_2$), 24.65 (dd, $^1J_{CP}$ = 7.6 Hz, $^3J_{CP}$ = 16.6 Hz, P*C*H$_2$), 29.73 (dd, $^1J_{CP}$ = 17.2 Hz, $^3J_{CP}$ = 31.0 Hz, P*C*H$_2$), 30.48 (s, C(*C*H$_3$)$_3$), 71.48 (dd, $^3J_{CP}$ = 2.4 Hz, $^3J_{CP}$ = 4.2 Hz, *C*(CH$_3$)$_3$). ^{31}P{^{1}H} NMR (121 MHz, $CDCl_3$, ppm): δ 1.97 (d, $^3J_{PP}$ = 7.0 Hz, *P*(CH$_3$)$_2$), 25.46 (d, $^3J_{PP}$ = 7.0 Hz, *P*(CH$_3$)$_2$). EA calcd for $C_{14}H_{34}Cl_2MoN_2P_2$ [%]: C, 36.61; H, 7.46; N, 6.10; found [%]: C, 36.96; H, 7.42; N, 6.19.

(t-BuN=)$_2$MoCl$_2$·(SIt-Bu) ***10***. A solution of **1** (0.371 g, 0.929 mmol) in 2 mL of diethyl ether was added dropwise to a solution of freshly distilled 1,3-*bis*(*tert*-butyl)imidazolin-2-ylidene (0.160 g, 0.878 mmol) in 5 mL of hexanes. The mixture was stirred for 2 hours resulting in a yellow precipitate. The supernate was decanted and the solids were washed with two, 2 mL portions of diethyl ether, and two, 2 mL portions of pentane. The solids were dried *in vacuo* yielding a pale-yellow powder of analytically pure **10**. Yield = 0.312 g (0.635 mmol, 72%). X-ray quality crystals were obtained after storing a saturated toluene solution, layered with pentane, at -30 ºC for 24 hours. ^{1}H NMR (300 MHz, C_6D_6, ppm): δ 1.52 (s, 18H, C(C*H*$_3$)$_3$), 1.60 (s, 18H, C(C*H*$_3$)$_3$), 2.80 (s, 4H, C*H*$_2$). ^{13}C{^{1}H} NMR (75 MHz, C_6D_6, ppm): δ 30.10 (C(*C*H$_3$)$_3$), 30.82 (C(*C*H$_3$)$_3$), 45.80 (*C*H$_2$), 56.62 (*C*(CH$_3$)$_3$), 72.15 (*C*(CH$_3$)$_3$), 212.39 (N*C*N). EA calcd for $C_{19}H_{40}Cl_2MoN_4$ [%]: C, 46.44; H, 8.20; N, 11.40; found [%]: C, 46.55; H, 8.18; N, 11.31.

Thermal Characterization. *Thermogravimetric Analysis.* TGA was performed on a TA Instruments Q500 instrument which was housed in a "chemical-free", nitrogen-filled (99.998%) MBraun glovebox. In a typical experiment 10.000 ± 1 mg of analyte was placed in a platinum pan and was heated to 500 ºC with a ramp rate of 10 ºC·min^{-1}, unless otherwise stated, using nitrogen (99.999% purity) as the purge gas. Langmuir vapor pressure equations were derived from TGA data using a previously reported method,[44] employing *bis*(2,2,6,6-tetramethyl-3,5-heptanedionato)copper(II) as the calibrant.[47] The TGA and vapor pressure curves for all compounds can be found in the SI.

Differential Scanning Calorimetry. DSC experiments were performed with a TA Instruments Q10 instrument. All DSC samples were hermetically sealed in aluminum pans, inside a glovebox prior to analysis. Due to the volatile nature of the analytes and their decomposition products, mass loadings greater than 1 mg often ruptured the sealed pans. Therefore, small mass loadings of 0.400 ± 0.1 mg were typically used for all DSC experiments. Unless otherwise stated all samples were heated to 400 ºC with a ramp rate of 10 ºC·min^{-1}, using nitrogen (99.998% purity) as the purge gas. The onset of decomposition (T_D) was defined as a 5% increase in exothermic heat flow from the baseline and all DSC plots are presented in the SI.

In Situ Thermolysis of ***2***. [(*t*-BuN=)$_2$MoCl$_2$]$_2$ (0.003 g, 0.005 mmol) was dissolved in 0.300 mL of C_6D_6 in a heavy-walled NMR tube. The NMR tube was flame-sealed, and the tube was left at room temperature for 18 hours to verify stoichiometry and stability. The NMR tube was stored in an oven at 170 ºC, in a sealed nitrogen-filled bottle (see Figure S34 for a photograph of the set up), and ^{1}H NMR spectra were collected, at room temperature, several times a day, for the first three days. It should be noted that the sample remained unchanged after 24 hours at 160 ºC. The NMR tube was stored upside-down in the oven because an insoluble orange material deposited on the inside walls of the tube, which affected the shimming. The starting material had completely disappeared, and the formation of isobutylene ceased, somewhere between 26 and 42 hours, at 170 ºC. After thermolysis: ^{1}H NMR (300 MHz, C_6D_6, ppm): δ 1.59 (t, 6H, $^4J_{HH}$ = 1.2 Hz, C*H*$_3$), 4.75 (sept, 2H, $^4J_{HH}$ = 1.2 Hz, C*H*$_2$). ^{13}C{^{1}H} NMR (75 MHz, C_6D_6, ppm): δ 24.11 (*C*H$_3$), 111.12 (*C*H$_2$), 141.98 (*C*=CH$_2$).

X-Ray Crystallography. The crystal chosen was attached to the tip of a MicroLoop with paratone-N oil. Measurements were made on a Bruker APEXII CCD equipped diffractometer (30 mA, 50 kV) using monochromated Mo Kα radiation (λ = 0.71073 Å) at 125 K.[48] The initial orientation and unit cell were indexed using a least-squares analysis of a random set of reflections collected from three series of 0.5° ω-scans, 10 seconds per frame and 12 frames per series, that were well distributed in reciprocal space. For most data collections, four ω-scan frame series were collected with 0.5° wide scans, 30 second frames and 366 frames per series at varying φ angles (φ = 0°, 90°, 180° and 270°). If 30 second frames were not used, the frame times are specified in the supporting information. The crystal to detector distance was set to 6 cm and a complete sphere of data was collected in every experiment. Cell refinement and data reduction were performed with the Bruker SAINT software,[49] which corrects for beam inhomogeneity, possible crystal decay, Lorentz and polarization effects. A multi-scan absorption correction was applied in all cases (SADABS).[50] The structures were solved using SHELXT-2014 and were refined using a full-matrix least-squares method on F^2 with SHELXL-2018.[51-53] The refinements were generally unremarkable. The non-hydrogen atoms were refined anisotropically. The hydrogen atoms bonded to carbon were included at geometrically idealized positions and were not refined. The isotropic thermal parameters of these hydrogen atoms were fixed at 1.2U_{eq} of the parent carbon atom or 1.5U_{eq} for methyl hydrogens. Specific details of individual refinements are given in the supporting information.

Associated Content

Supporting Information

The Supporting Information is available free of charge on the ACS Publications website at DOI:

NMR spectra, DSC curves, TGA plots, and vapor pressure estimates modeled using the Langmuir equation, for all compounds discussed herein, can be found in the SI. Additional crystallographic details and images are also found therein. Finally, kinetic data for the *in situ* thermolysis of **2**, and EDS analyses are also included (PDF).

Crystallographic information files for compounds **1**, **2**, **4**, & **6**–**10** were also deposited at the CCDC (1944212-1944219) (CIF).

Author Information

Corresponding Author

*E-mail: Michael.land@carleton.ca

ORCID

Michael A. Land: 0000-0001-5861-242X
Katherine N. Robertson: 0000-0002-5602-8059
Seán T. Barry: 0000-0001-5515-4734

Author Contributions

The manuscript was written through contributions of all authors. All authors have given approval to the final version of the manuscript.

Acknowledgements

MAL thanks the Ontario Graduate Scholarship (OGS) Program, Fluorosense Inc, and Carleton University for financial support. Funding for KNR was provided by Prof. Jason Clyburne at Saint Mary's University (SMU). STB acknowledges the Natural Sciences and Engineering Research Council of Canada (NSERC, RGPIN-2019-06213). We also acknowledge Joseph Zurakowski for preparing SI*t*-Bu, Matthew Griffiths for assistance with EDS, and Sharon Curtis, at University of Ottawa, for HRMS acquisition. Finally, we thank Patricia Granados (SMU) for technical support with EA, and Prof. Jason Masuda (SMU) for providing access to a glovebox to prepare samples for EA.

Abbreviations

ALD, atomic layer deposition; bpy, 2,2'-bipyridine; dme, 1,2-dimethoxyethane; dmpe, 1,2-*bis*(dimethylphosphino)ethane; DSC, differential scanning calorimetry; ESD, energy dispersive X-ray spectroscopy; py, pyridine; SI*t*-Bu, 1,3-*bis*(*tert*-butyl)imidazolin-2-ylidene; TGA, thermogravimetric analysis; TMEDA, *N*,*N*,*N'*,*N'*-tetramethylethylenediamine.

References

(1) Hau-Riege, C. S. An Introduction to Cu Electromigration. *Microelectron. Reliab.* **2004**, *44*, 195–205.

(2) Adelmann, C.; Wen, L. G.; Peter, A. P.; Siew, Y. K.; Croes, K.; Swerts, J.; Popovici, M.; Sankaran, K.; Pourtois, G.; Van Elshocht, S.; Bömmels, J.; Tökei, Z. Alternative Metals for Advanced Interconnects. In *IEEE International Interconnect Technology Conference*; IEEE, 2014; 173–176.

(3) Miikkulainen, V.; Leskelä, M.; Ritala, M.; Puurunen, R. L. Crystallinity of Inorganic Films Grown by Atomic Layer Deposition: Overview and General Trends. *J. Appl. Phys.* **2013**, *113*, 021301.

(4) Barry, S. T. Amidinates, Guanidinates and Iminopyrrolidinates: Understanding Precursor Thermolysis to Design a Better Ligand. *Coord. Chem. Rev.* **2013**, *257*, 3192–3201.

(5) Juppo, M.; Vehkamäki, M.; Ritala, M.; Leskelä, M. Deposition of Molybdenum Thin Films by an Alternate Supply of $MoCl_5$ and Zn. *J. Vac. Sci. Technol., A* **1998**, *16*, 2845–2850.

(6) Seghete, D.; Rayner, G. B.; Cavanagh, A. S.; Anderson, V. R.; George, S. M. Molybdenum Atomic Layer Deposition Using MoF_6 and Si_2H_6 as the Reactants. *Chem. Mater.* **2011**, *23*, 1668–1678.
(7) Bertuch, A.; Sundaram, G.; Saly, M.; Moser, D.; Kanjolia, R. Atomic Layer Deposition of Molybdenum Oxide Using Bis(Tert-Butylimido)Bis(Dimethylamido) Molybdenum. *J. Vac. Sci. Technol., A* **2014**, *32*, 01A119.
(8) Miikkulainen, V.; Suvanto, M.; Pakkanen, T. A. Atomic Layer Deposition of Molybdenum Nitride from Bis(Tert -Butylimido)-Bis(Dimethylamido)Molybdenum and Ammonia onto Several Types of Substrate Materials with Equal Growth per Cycle. *Chem. Mater.* **2007**, *19*, 263–269.
(9) Miikkulainen, V.; Suvanto, M.; Pakkanen, T. A. Bis(Tert-Butylimido)-Bis(Dialkylamido) Complexes of Molybdenum as Atomic Layer Deposition (ALD) Precursors for Molybdenum Nitride: The Effect of the Alkyl Group. *Chem. Vap. Depos.* **2008**, *14*, 71–77.
(10) Miikkulainen, V.; Suvanto, M.; Pakkanen, T. A. Molybdenum Nitride Nanotubes. *Thin Solid Films* **2008**, *516*, 6041–6047.
(11) Miikkulainen, V.; Suvanto, M.; Pakkanen, T. A.; Siitonen, S.; Karvinen, P.; Kuittinen, M.; Kisonen, H. Thin Films of MoN, WN, and Perfluorinated Silane Deposited from Dimethylamido Precursors as Contamination Resistant Coatings on Micro-Injection Mold Inserts. *Surf. Coatings Technol.* **2008**, *202*, 5103–5109.
(12) Macco, B.; Vos, M. F. J.; Thissen, N. F. W.; Bol, A. A.; Kessels, W. M. M. Low-Temperature Atomic Layer Deposition of MoOx for Silicon Heterojunction Solar Cells. *Phys. Status Solidi RRL* **2015**, *9*, 393–396.
(13) Ziegler, J.; Mews, M.; Kaufmann, K.; Schneider, T.; Sprafke, A. N.; Korte, L.; Wehrspohn, R. B. Plasma-Enhanced Atomic-Layer-Deposited MoOx Emitters for Silicon Heterojunction Solar Cells. *Appl. Phys. A* **2015**, *120*, 811–816.
(14) Vos, M. F. J.; Macco, B.; Thissen, N. F. W.; Bol, A. A.; Kessels, W. M. M. Atomic Layer Deposition of Molybdenum Oxide from $(NtBu)_2(NMe_2)_2Mo$ and O_2 Plasma. *J. Vac. Sci. Technol., A* **2016**, *34*, 01A103.
(15) Keller, B. D.; Bertuch, A.; Provine, J.; Sundaram, G.; Ferralis, N.; Grossman, J. C. Process Control of Atomic Layer Deposition Molybdenum Oxide Nucleation and Sulfidation to Large-Area MoS_2 Monolayers. *Chem. Mater.* **2017**, *29*, 2024–2032.
(16) Wei, Z.; Hai, Z.; Akbari, M. K.; Qi, D.; Xing, K.; Zhao, Q.; Verpoort, F.; Hu, J.; Hyde, L.; Zhuiykov, S. Atomic Layer Deposition-Developed Two-Dimensional α-MoO_3 Windows Excellent Hydrogen Peroxide Electrochemical Sensing Capabilities. *Sensors Actuators B Chem.* **2018**, *262*, 334–344.
(17) Xu, H.; Akbari, M. K.; Hai, Z.; Wei, Z.; Hyde, L.; Verpoort, F.; Xue, C.; Zhuiykov, S. Ultra-Thin MoO_3 Film Goes Wafer-Scaled Nano-Architectonics by Atomic Layer Deposition. *Mater. Des.* **2018**, *149*, 135–144.
(18) Sharma, A.; Verheijen, M. A.; Wu, L.; Karwal, S.; Vandalon, V.; Knoops, H. C. M.; Sundaram, R. S.; Hofmann, J. P.; Kessels, W. M. M.; Bol, A. A. Low-Temperature Plasma-Enhanced Atomic Layer Deposition of 2-D MoS_2: Large Area, Thickness Control and Tuneable Morphology. *Nanoscale* **2018**, *10*, 8615–8627.
(19) Kalanyan, B.; Beams, R.; Katz, M. B.; Davydov, A. V.; Maslar, J. E.; Kanjolia, R. K. MoS_2 Thin Films from a $(NtBu)_2(NMe_2)_2Mo$ and 1-Propanethiol Atomic Layer Deposition Process. *J. Vac. Sci. Technol., A* **2019**, *37*, 010901.
(20) Bertuch, A.; Keller, B. D.; Ferralis, N.; Grossman, J. C.; Sundaram, G. Plasma Enhanced

Atomic Layer Deposition of Molybdenum Carbide and Nitride with Bis(Tert-Butylimido)Bis(Dimethylamido) Molybdenum. *J. Vac. Sci. Technol., A* **2017**, *35*, 01B141.
(21) Dyer, P. W.; Gibson, V. C.; Howard, J. A. K.; Whittle, B.; Wilson, C. Four Coordinate Bis(Imido) Alkene Complexes of Molybdenum(IV): Relatives of the Zirconocene Family. *J. Chem. Soc. Chem. Commun.* **1992**, *04* , 1666–1668.
(22) Fox, H. H.; Yap, K. B.; Robbins, J.; Cai, S.; Schrock, R. R. Simple-High Yield Syntheses of Molybdenum(VI) Bis(Imido) Complexes of the Type $Mo(NR)_2Cl_2$(1,2-Dimethoxyethane). *Inorg. Chem.* **1992**, *31*, 2287–2289.
(23) Thiede, T.; Gwildies, V.; Alsamann, L.; Rische, D.; Fischer, R. Novel Precursors for the MOCVD of Molybdenum Nitride. *ECS Transactions* **2009**, *25*, 593–600.
(24) Mattinen, M.; Wree, J.-L.; Stegmann, N.; Ciftyurek, E.; Achhab, M. El; King, P. J.; Mizohata, K.; Räisänen, J.; Schierbaum, K. D.; Devi, A.; et al. Atomic Layer Deposition of Molybdenum and Tungsten Oxide Thin Films Using Heteroleptic Imido-Amidinato Precursors: Process Development, Film Characterization, and Gas Sensing Properties. *Chem. Mater.* **2018**, *30*, 8690–8701.
(25) Lichtscheidl, A. G.; Ng, V. W. L.; Müller, P.; Takase, M. K.; Schrock, R. R. Molybdenum Monoaryloxide Pyrrolide Alkylidene Complexes That Contain Mono-Ortho-Substituted Phenyl Imido Ligands. *Organometallics* **2012**, *31*, 2388–2394.
(26) Hering, F.; Varga, P.; Würtemberger, M.; Radius, U. Bisimido Molybdenum Complexes of the Extremely Bulky Pr* Framework. *Z. Anorg. Allg. Chem.* **2015**, *641*, 2530–2535.
(27) Chiu, H.-T.; Chang, G.-B.; Ho, W.-Y.; Chuang, S.-H.; Lee, G.-H.; Peng, S.-M. Syntheses and X-Ray Crystal Structures of Dichlorobis(Tert-Butylimido) Complexes of Molybdenum(VI); Potential Precursors to Molybdenum Nitride and Molybdenum Carbonitride. *J. Chinese Chem. Soc.* **1994**, *41*, 755–761.
(28) Danopoulos, A. A.; Leung, W.-H.; Wilkinson, G.; Hussain-Bates, B.; Hursthouse, M. B. T-Butylimido Complexes of Chromium. X-Ray Crystal Structures of $Cr(NBut)_2(PMe_2Ph)Cl_2$ and $[Cr(NBut)_2(C_5H_4N)_2(\eta1\text{-}O_3SCF_3)]O_3SCF_3$. *Polyhedron* **1990**, *9*, 2625–2634.
(29) Danopoulos, A. A.; Wilkinson, G.; Sweet, T. K. N.; Hursthouse, M. B. Arylimido Complexes of Chromium-(VI), -(V) and -(IV). *J. Chem. Soc. Dalt. Trans.* **1995**, 2111–2123.
(30) Nugent, W. A. Synthesis of Some d0 Organoimido Complexes of the Early Transition Metals. *Inorg. Chem.* **1983**, *22*, 965–969.
(31) Schoettel, G.; Kress, J.; Osborn, J. A. A Simple Route to Molybdenum-Carbene Catalysts for Alkene Metathesis. *J. Chem. Soc. Chem. Commun.* **1989**, 1062–1063.
(32) Dreisch, K.; Andersson, C.; StÅlhandske, C. Reactions of $[WO_2Cl_2(dme)]$ with Tert.Butyltrimethylsilyalmine—x-ray Structure of $[W(NBut)_2Cl_2$(But-dab)] (But-dab = N,N′-Dit-t-Butyl-1,4-Diaza-1,3-Butadiene). *Polyhedron* **1993**, *12*, 1335–1343.
(33) Chan, M. C. W.; Lee, F.; Cheung, K.; Che, C. Synthetic, Structural and Electrochemical Studies of Cationic Chromium(VI) and Molybdenum(VI) Bis(Imido) Complexes Supported by 1,4,7-Triazacyclononane Macrocycles. *J. Chem. Soc. Dalt. Trans.* **1999**, 3197–3201.
(34) Herrmann, W. A.; Thiel, W. R.; Herdtweck, E. Synthesen Und Strukturen Neuer Komplexes Des 2,2′-Bipyridins Mit Niob, Molybdän, Wolfram Und Rhenium in Hohen Oxidationsstufen. *Chem. Ber.* **1990**, *123* , 271–276.
(35) Griffiths, M. B. E.; Pallister, P. J.; Mandia, D. J.; Barry, S. T. Atomic Layer Deposition of Gold Metal. *Chem. Mater.* **2016**, *28*, 44–46.
(36) Griffiths, M. B. E.; Dubrawski, Z. S.; Bačić, G.; Masuda, J. D.; Japahuge, A.; Zeng, T.; Barry, S. T. Controlling Thermal Stability and Volatility of Organogold(I) Compounds for

Vapor Deposition with Complementary Ligand Design. *ChemRxiv*. Preprint. May 2019.
(37) Coyle, J. P.; Sirianni, E. R.; Korobkov, I.; Yap, G. P. A.; Dey, G.; Barry, S. T. Study of Monomeric Copper Complexes Supported by N -Heterocyclic and Acyclic Diamino Carbenes. *Organometallics* **2017**, *36*, 2800–2810.
(38) Coyle, J. P.; Dey, G.; Sirianni, E. R.; Kemell, M. L.; Yap, G. P. A.; Ritala, M.; Leskelä, M.; Elliott, S. D.; Barry, S. T. Deposition of Copper by Plasma-Enhanced Atomic Layer Deposition Using a Novel N-Heterocyclic Carbene Precursor. *Chem. Mater.* **2013**, *25*, 1132–1138.
(39) Arentsen, K.; Caddick, S.; Cloke, F. G. N. On the Efficiency of Two-Coordinate Palladium(0) N-Heterocyclic Carbene Complexes in Amination and Suzuki-Miyaura Reactions of Aryl Chlorides. *Tetrahedron* **2005**, *61*, 9710–9715.
(40) Barrie, P.; Coffey, T. A.; Forster, G. D.; Hogarth, G. Bent vs. Linear Imido Ligation at the Octahedral Molybdenum(VI) Dithiocarbamate Stabilised Centre. *J. Chem. Soc. Dalt. Trans.* **1999**, 4519–4528.
(41) Addison, A. W.; Rao, T. N.; Reedijk, J.; van Rijn, J.; Verschoor, G. C. Synthesis, Structure, and Spectroscopic Properties of Copper(II) Compounds Containing Nitrogen–Sulphur Donor Ligands; the Crystal and Molecular Structure of Aqua[1,7-Bis(N-Methylbenzimidazol-2′-Yl)-2,6-Dithiaheptane]Copper(II) Perchlorate. *J. Chem. Soc., Dalt. Trans.* **1984**, 1349–1356.
(42) Nugent, W. A.; Harlow, R. L. Reaction of Group 6 Organoimido Complexes with Organozinc. Reductive Elimination across a Metal-Nitrogen Multiple Bond. *J. Am. Chem. Soc.* **1980**, *102*, 1759–1760.
(43) Buchmeiser, M. R.; Sen, S.; Unold, J.; Frey, W. N-Heterocyclic Carbene, High Oxidation State Molybdenum Alkylidene Complexes: Functional-Group-Tolerant Cationic Metathesis Catalysts. *Angew. Chemie Int. Ed.* **2014**, *53*, 9384–9388.
(44) Kunte, G. V.; Shivashankar, S. A.; Umarji, A. M. Thermogravimetric Evaluation of the Suitability of Precursors for MOCVD. *Meas. Sci. Technol.* **2008**, *19*, 025704.
(45) Coyle, J. P.; Kurek, A.; Pallister, P. J.; Sirianni, E. R.; Yap, G. P. A.; Barry, S. T. Preventing Thermolysis: Precursor Design for Volatile Copper Compounds. *Chem. Commun.* **2012**, *48*, 10440.
(46) Edwards, D. A.; Fowles, G. W. A. Ammonolysis of Molybdenum(V) Chloride. *J. Less-Common Met.* **1961**, *3*, 181–187.
(47) Colominas, C.; Lau, K. H.; Hildenbrand, D. L.; Crouch-Baker, S.; Sanjurjo, A. Vapor Pressures of the Copper and Yttrium β-Diketonate MOCVD Precursors. *J. Chem. Eng. Data* **2001**, *46*, 446–450.
(48) APEX II (Bruker, 2008) Bruker AXS Inc., Madison, Wisconsin, USA.
(49) SAINT (Bruker, 2008) Bruker AXS Inc., Madison, Wisconsin, USA.
(50) SADABS (Bruker, 2008) Bruker AXS Inc., Madison, Wisconsin, USA.
(51) Sheldrick, G. M. A Short history of SHELX. *Acta Cryst. A* **2008**, *64*, 112-122.
(52) Sheldrick, G. M. SHELXT - Integrated space-group and crystal-structure determination. *Acta Cryst. A* **2015**, *71*, 3-8.
(53) Sheldrick, G. M. Crystal structure refinement with SHELXL. *Acta Cryst. C* **2015**, *71*, 3-8.